

# RadioDiff- $k^2$ : Helmholtz Equation Informed Generative Diffusion Model for Multi-Path Aware Radio Map Construction

Xiucheng Wang,  Graduate Student Member, IEEE, Qiming Zhang,  Nan Cheng,  Senior Member, IEEE, Ruijin Sun,  Member, IEEE, Zan Li,  Fellow, IEEE, Shuguang Cui,  Fellow, IEEE, and Xuemin (Sherman) Shen,  Fellow, IEEE

**Abstract**—In this paper, we propose a novel physics-informed generative learning approach, termed RadioDiff- $k^2$ , for accurate and efficient multipath-aware radio map (RM) construction. As wireless communication evolves towards environment-aware paradigms, driven by the increasing demand for intelligent and proactive optimization in sixth-generation (6G) networks, accurate construction of RMs becomes crucial yet highly challenging. Conventional electromagnetic (EM)-based methods, such as full-wave solvers and ray-tracing approaches, exhibit substantial computational overhead and limited adaptability to dynamic scenarios. Although, existing neural network (NN) approaches have efficient inferencing speed, they lack sufficient consideration of the underlying physics of EM wave propagation, limiting their effectiveness in accurately modeling critical EM singularities induced by complex multipath environments. To address these fundamental limitations, we propose a novel physics-inspired RM construction method guided explicitly by the Helmholtz equation, which inherently governs EM wave propagation. Specifically, we theoretically establish a direct correspondence between EM singularities, which correspond to the critical spatial features influencing wireless propagation, and regions defined by negative wave numbers in the Helmholtz equation. Based on this insight, we design an innovative dual generative diffusion model (DM) framework comprising one DM dedicated to accurately inferring EM singularities and another DM responsible for reconstructing the complete RM using these singularities along with environmental contextual information. Our physics-informed approach uniquely combines the efficiency advantages of data-driven methods with rigorous physics-based EM modeling, significantly enhancing RM accuracy, particularly in complex propagation environments dominated by multipath effects.

**Index Terms**—Radio map, physics-informed neural network,

Helmholtz equation, generative artificial intelligence, diffusion model.

## I. INTRODUCTION

The paradigm shift in wireless communication from environment-independent operation to an environment-aware framework marks a fundamental transformation in the design and functionality of next-generation networks [1], [2]. This transition is driven by the increasing demand for intelligent, adaptive, and context-aware communication systems, particularly in the era of 6G networks, where network nodes must not only operate within but also dynamically interact with complex and time-varying environments [3], [4]. A fundamental enabler of this transformation is the radio map (RM), which provides a spatial representation of critical wireless channel characteristics, including path loss, angle of arrival (AoA), and interference distribution [5]. By integrating location-specific channel state information (CSI), RMs facilitate proactive network optimization, intelligent resource allocation, and real-time adaptation to environmental dynamics, offering a significant advantage over conventional reactive network management strategies [6]. One of the most impactful applications of RM lies in low-overhead channel estimation, where it enables infrastructure components, such as intelligent reflecting surfaces (IRS) and massive multiple-input multiple-output (MIMO) systems, to obtain high-fidelity CSI with minimal reliance on pilot signals [7]. This reduces training overhead, mitigates pilot contamination, and enhances spectral efficiency, making RM a cornerstone for sustainable and scalable 6G wireless communication. Furthermore, RM plays a pivotal role in the trajectory planning, coverage optimization, and interference mitigation of mobile network elements, such as autonomous aerial vehicles (AAVs) and satellites in space-air-ground integrated networks (SAGIN) [8], [9]. By precomputing the spatial variations of wireless channel properties, RM allows mobile nodes to anticipate and mitigate signal blockages, optimize handovers, and enhance connectivity resilience in highly dynamic environments.

However, the construction of RM is inherently challenging due to the simultaneous demands for efficiency and accuracy, particularly within highly dynamic 6G environments [5]. Broadly, RM construction methods can be categorized

This work was supported by the National Key Research and Development Program of China (2024YFB907500).

Xiucheng Wang, Qiming Zhang, Nan Cheng, Ruijin Sun, and Zan Li are with the State Key Laboratory of ISN and School of Telecommunications Engineering, Xidian University, Xi'an 710071, China (e-mail: xcwang\_1@stu.xidian.edu.cn; dr.nan.cheng@ieee.org; {sunruijin, zanli}@xidian.edu.cn). *Nan Cheng is the corresponding author.*

Qiming Zhang is with the School of Artificial Intelligence, Xidian University, Xi'an 710071, China (e-mail: 23009200991@stu.xidian.edu.cn);

Shuguang Cui is with the School of Science and Engineering (SSE), Shenzhen Future Network of Intelligence Institute (FNii-Shenzhen), and Guangdong Provincial Key Laboratory of Future Networks of Intelligence, The Chinese University of Hong Kong (Shenzhen), Shenzhen, China (e-mail: shuguangcui@cuhk.edu.cn);

Xuemin (Sherman) Shen is with the Department of Electrical and Computer Engineering, University of Waterloo, Waterloo, N2L 3G1, Canada (e-mail: sshen@uwaterloo.ca).

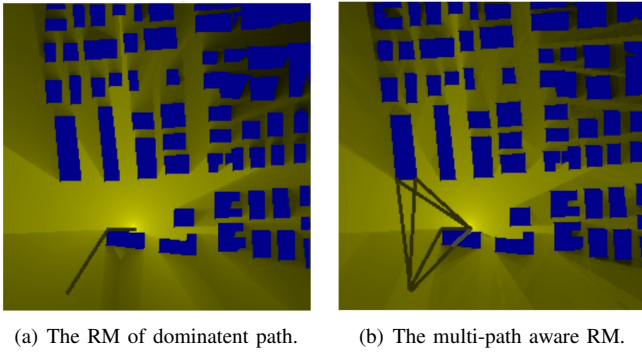


Fig. 1: Illustration of the RM, where (a) is the RM only considering the dominating path, (b) is the RM considering the multi-path effect, and the propagating path is shown for a specific location.

into two distinct classes: electromagnetic (EM)-based high-precision methods [14] and data-driven approaches emphasizing computational efficiency [12]. Traditional high-precision EM-based methods rely on solving Maxwell’s equations via full-wave numerical simulations, providing highly accurate spatial distributions of wireless channel characteristics [15]. However, their computational complexity is substantial, typically requiring hours to simulate EM wave propagation even within meter-scale scenarios [14]. To mitigate computational demands, approximate methods such as ray-tracing techniques have emerged, significantly reducing the required time to tens of minutes for kilometer-scale RM generation by simplifying EM wave propagation laws [16]. However, these EM-based approaches inherently assume a static environment during the computation period; this assumption is incompatible with the temporally and spatially dynamic characteristics of 6G networks, which include mobile network elements such as AAVs and satellites [17]. Consequently, recent attention has shifted toward neural network (NN)-based data-driven methods, offering efficiency through their rapid inference capabilities [10], [12], [13]. Nonetheless, existing NN-based approaches encounter significant limitations, notably their inability to accurately capture electromagnetic singularities resulting from intricate EM-environment interactions, as is shown in Fig. 2. These singularities, characterized by abrupt spatial variations in channel properties like pathloss, critically impact network performance by influencing factors such as user signal quality, AAV trajectory design, and beamforming alignment [9]. Moreover, traditional NN architectures, originally designed for tasks such as image processing or pattern recognition, inadequately address the physical nature and complexity of EM singularities, as these singularities are intrinsically tied to the physics of wave propagation rather than visual patterns or frequency domain characteristics [12]. An additional fundamental shortcoming of existing data-driven methods is their predominant focus on modeling the main propagation path, largely neglecting the complex yet critical multipath phenomena inherent in real-world wireless communication environments. Multipath propagation leads to numerous secondary signals arriving at the receiver from various directions and with diverse

delays, significantly complicating the spatial distribution of EM singularities. Moreover, as shown in Fig. 3, even classical digital filtering techniques fail to recover these fine-scale multipath-induced patterns [18], further underscoring the limitations of existing approaches. These observations highlight the urgent need for a new class of RM construction methods that not only infer the spatial distribution of channel characteristics but also incorporate a deep understanding of the physical mechanisms, particularly the multipath-driven singularities underpinning wave propagation.

However, achieving both efficiency and accuracy in RM construction remains challenging, motivating the development of novel methods to bridge the gap between the high precision of physics-based approaches and the computational efficiency of data-driven techniques. To address this challenge, this paper proposes a physics-inspired theoretical framework for effectively modeling the spatial distribution features of EM wave propagation. By explicitly incorporating the physics embedded in the EM wave equation, particularly the Helmholtz equation [15], into the NN training process, our method enables the NN to capture spatial distribution characteristics intrinsic to EM wave propagation. Specifically, through rigorous theoretical analysis of the Helmholtz equation, we discover that electromagnetic singularities, which are key regions exhibiting abrupt changes in wireless channel features due to multipath effects, directly correspond to regions characterized by a complex wave number where  $k^2 < 0$ . Leveraging this novel insight, we devise a specialized NN architecture and training strategy that significantly enhances the NN’s capability to identify and model abrupt variations in wireless channel characteristics caused by multipath propagation. Moreover, inspired by the success of the generative diffusion model (DM) [19] for RM construction. The generative DM is used as the backbone to achieve a high performance. Consequently, our physics-informed approach bridges the critical gap between traditional data-driven models and the underlying physical principles governing EM propagation, significantly advancing the accuracy and reliability of RM construction in complex 6G communication scenarios. The main contributions in this paper are summarized as follows.

- 1) Theoretically, a physics-inspired RM construction theory is proposed in this paper, which explicitly integrates the underlying EM propagation characteristics governed by the Helmholtz equation into NN learning frameworks. Through an in-depth theoretical analysis of the Helmholtz equation, we reveal that electromagnetic singularities, corresponding to abrupt spatial variations in the wireless channel caused by multipath propagation, are characterized by regions where the  $k^2 < 0$ . This insight fundamentally enhances the ability of NNs to accurately capture and predict intricate spatial features, significantly improving the accuracy of RM-based wireless environmental awareness required by next-generation communication systems.
- 2) Based on the physics-informed theory, we propose an innovative dual DM-based RM construction method specifically tailored for effectively modeling the complex

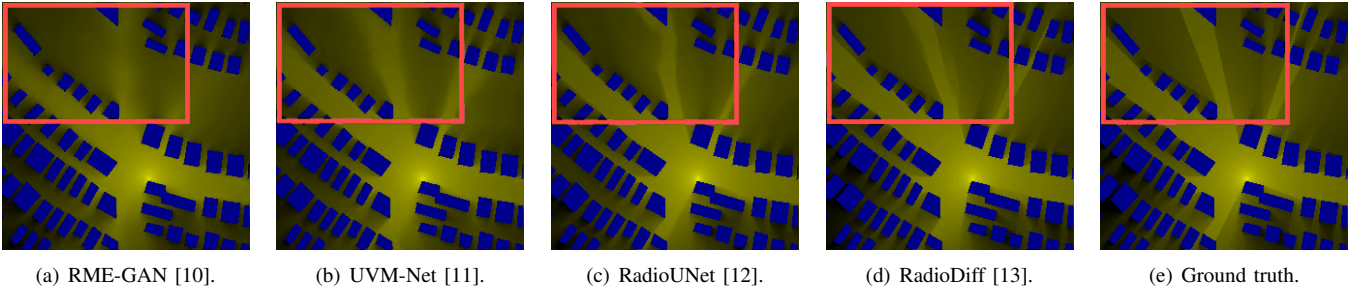


Fig. 2: Illustration of RMs constructed by various NN-based baseline methods, where RadioDiff is the SOTA NN-based RM construction method. The results indicate that existing NN-based approaches exhibit limited capability in capturing fine-grained texture features of the RM, particularly those associated with abrupt spatial variations in wireless channel characteristics. This deficiency hinders the ability of these methods to reliably detect electromagnetic singularities, thereby limiting their effectiveness in downstream wireless network optimization tasks.

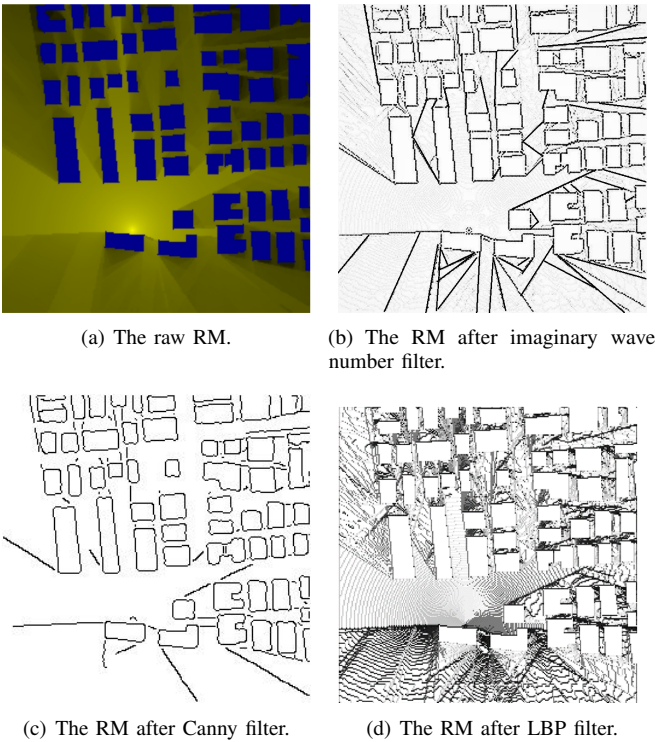


Fig. 3: Illustration of the different texture extraction methods.

multipath propagation environment. In our architecture, the first DM is explicitly designed and trained to predict the spatial distribution of EM singularities. The second NN leverages these learned singularities together with environmental context to accurately reconstruct the RM. This novel dual-stage DM approach ensures that intricate propagation characteristics induced by multipath effects are meticulously captured and effectively translated into the final RM.

- 3) Different from traditional NN-based RM methods that primarily model the main path propagation features, our proposed method explicitly addresses multipath effects. By comprehensively incorporating multipath-induced singularities into RM construction, our method is particularly advantageous in highly dynamic and complex 6G scenarios.

- 4) Extensive experimental results demonstrate that our physics-informed NN significantly outperforms existing state-of-the-art approaches, validating its superior capability in accurately capturing critical EM singularities and complex spatial propagation features. The proposed method not only achieves remarkable improvements in widely adopted evaluation metrics, such as normalized mean square error (NMSE), root mean square error (RMSE), structural similarity (SSIM), and peak signal-to-noise ratio (PSNR), but also establishes a new state-of-the-art baseline for RM construction tasks. These outcomes underscore the efficacy and innovation of our physics-informed approach in realizing robust and accurate radio maps essential for intelligent, proactive 6G wireless network management.

## II. RELATED WORKS AND PRELIMINARIES

### A. Related Works

RM construction methods can generally be classified into sampling-based and sampling-free approaches. Sampling-based methods rely on sparse pathloss measurements (SPM) collected at specific locations, which are then interpolated to estimate the RM over the entire area. These methods do not require prior knowledge of the environment or base station (BS) locations. Classic techniques include K-nearest neighbors (KNN) interpolation, which estimates unknown values by a weighted average of nearby measurements [20], and local multinomial regression, which fits a local linear model via least-squares minimization using nearby data points [21]. More sophisticated techniques such as Kriging treat the interpolation as a stochastic process governed by spatial correlation, allowing for more accurate pathloss prediction by modeling the covariance structure of measurements [22].

Despite their simplicity, these methods suffer from two core limitations: a strong dependence on the availability of SPM and limited reconstruction accuracy, particularly in regions with sparse measurements or complex propagation environments [12], [23]. As a result, sampling-free RM construction has gained increasing attention. These approaches eliminate the need for measurement data in the target area and instead leverage environmental features—such as obstacle positions,

heights, and BS coordinates—to infer location-specific channel information. Representative efforts include RadioUNet, which adapts the U-Net architecture from image-to-image translation tasks to RM generation using MSE-based supervision [12], and RadioNet, which incorporates transformer-based attention mechanisms to capture global spatial dependencies in RM construction [23]. Further, graph neural networks (GNNs) have been applied to exploit the relational structure of spatial layouts for more expressive modeling [24]. While these methods offer improvements, most treat RM construction as a purely discriminative learning task and may struggle to capture the full distributional complexity of pathloss patterns in dynamic wireless environments. Some attempts, such as RME-GAN, introduced generative frameworks based on generative adversarial networks (GANs) to enhance output realism [10]. However, RME-GAN remains dependent on sparse measurements, thus not truly sampling-free. In contrast, this work frames RM construction as a conditional generative modeling task, proposing a diffusion-based method that generates high-fidelity RMs solely from environmental and BS input features—without relying on sampling within the target region. This fundamentally shifts the RM construction paradigm, enabling stronger generalization and distribution modeling capabilities.

### B. Score-Based Denoising Diffusion Model

DMs have recently emerged as powerful generative frameworks capable of capturing complex data distributions and synthesizing high-fidelity samples [19]. Among these, score-based diffusion models define a generative process grounded in stochastic differential equations (SDEs), wherein data undergoes progressive corruption and is later reconstructed by learning to approximate the gradient of the data log-likelihood, known as the score function [25]. Unlike classical DMs that adopt discrete Markov chains for the forward and reverse noise processes, score-based models perturb data in continuous time via SDEs, making them well-suited for solving inverse problems such as radio map reconstruction through Bayesian sampling principles. The forward process is formulated by the SDE as follows.

$$d\mathbf{x} = \mathbf{f}(\mathbf{x}, t)dt + g(t)d\mathbf{w}, \quad (1)$$

where  $\mathbf{f}(\mathbf{x}, t)$  denotes the drift component,  $g(t)$  is a time-dependent diffusion coefficient, and  $d\mathbf{w}$  is a Wiener process. As time  $t$  increases, the data distribution  $p_t(\mathbf{x})$  transitions toward an isotropic Gaussian. Reconstructing the original data entails solving the reverse-time SDE as follows.

$$d\mathbf{x} = [\mathbf{f}(\mathbf{x}, t) - g^2(t)\nabla_{\mathbf{x}} \log p_t(\mathbf{x})] dt + g(t)d\bar{\mathbf{w}}, \quad (2)$$

where  $\nabla_{\mathbf{x}} \log p_t(\mathbf{x})$  is the score function, typically approximated by a neural network  $s_{\theta}(\mathbf{x}, t)$ . The objective is to train  $s_{\theta}$  as follows.

$$s_{\theta}(\mathbf{x}, t) \approx \nabla_{\mathbf{x}} \log p_t(\mathbf{x}). \quad (3)$$

For deterministic sampling, an equivalent probability flow ODE is derived:

$$d\mathbf{x} = \left[ \mathbf{f}(\mathbf{x}, t) - \frac{1}{2}g^2(t)\nabla_{\mathbf{x}} \log p_t(\mathbf{x}) \right] dt, \quad (4)$$

which allows sample generation without stochasticity, analogous to denoising diffusion probabilistic models (DDPMs). In DDPMs, the forward noise process is discretized as follows.

$$q(\mathbf{x}_t | \mathbf{x}_{t-1}) = \mathcal{N}(\mathbf{x}_t; \alpha_t \mathbf{x}_{t-1}, \beta_t \mathbf{I}), \quad (5)$$

and the score is estimated via a learned denoiser  $\epsilon_{\theta}$  as follows.

$$s_{\theta}(\mathbf{x}, t) = -\frac{\epsilon_{\theta}(\mathbf{x}, t)}{\sqrt{1 - \alpha_t}}. \quad (6)$$

This formulation highlights DDPM as a discrete approximation of continuous score-based models using a variance-preserving scheme.

In the context of RM construction, decoupled diffusion models (DDMs) have been proposed to improve generative stability, particularly in the RadioDiff framework [26]. Unlike standard models that inject noise directly, DDM first attenuates the original input to a zero baseline, followed by noise injection. The forward transition from  $\mathbf{x}_0$  to  $\mathbf{x}_t$  is governed as follows.

$$q(\mathbf{x}_t | \mathbf{x}_0) = \mathcal{N}(\gamma_t \mathbf{x}_0, \delta_t^2 \mathbf{I}), \quad (7)$$

with time-dependent coefficients  $\gamma_t$  and  $\delta_t$  controlling signal decay and noise variance. The process is further described by the SDE as follows.

$$d\mathbf{x}_t = \mathbf{f}_t \mathbf{x}_t dt + g_t d\epsilon_t, \quad (8)$$

$$\mathbf{f}_t = \frac{d \log \gamma_t}{dt}, \quad (9)$$

$$\int_0^t \mathbf{f}_t dt = -\mathbf{x}_0 \quad (10)$$

$$g_t^2 = \frac{d\delta_t^2}{dt} - 2\mathbf{f}_t \delta_t^2, \quad (11)$$

where  $\mathbf{f}_t$  dictates attenuation rate and  $g_t^2$  captures noise accumulation over time.

The reverse-time generation process reconstructs  $\mathbf{x}_0$  from  $\mathbf{x}_t$  by solving following equation.

$$d\mathbf{x}_t = [\mathbf{f}_t \mathbf{x}_t - g_t^2 \nabla_{\mathbf{x}} \log q(\mathbf{x}_t)] dt + g_t d\bar{\epsilon}_t. \quad (12)$$

Thanks to its two-phase design, DDM stabilizes training and improves sampling quality by decoupling data transformation and noise injection. The deterministic transformation toward the zero vector simplifies forward sampling as follows.

$$q(\mathbf{x}_t | \mathbf{x}_0) = \mathcal{N}\left(\mathbf{x}_0 + \int_0^t \mathbf{f}_{\tau} d\tau, t\mathbf{I}\right), \quad (13)$$

and enables an efficient reverse update as follows.

$$q(\mathbf{z}_{t-\Delta t} | \mathbf{z}_t, \mathbf{z}_0) = \mathcal{N}\left(\mathbf{z}_t + \int_t^{t-\Delta t} \mathbf{f}_t dt - \frac{\Delta t}{\sqrt{t}} \boldsymbol{\epsilon}, \frac{\Delta t(t - \Delta t)}{t} \mathbf{I}\right). \quad (14)$$

Through this structured perturbation mechanism, DDM enhances generation quality and computational efficiency, making it especially suitable for high-fidelity RM reconstruction in next-generation wireless networks.

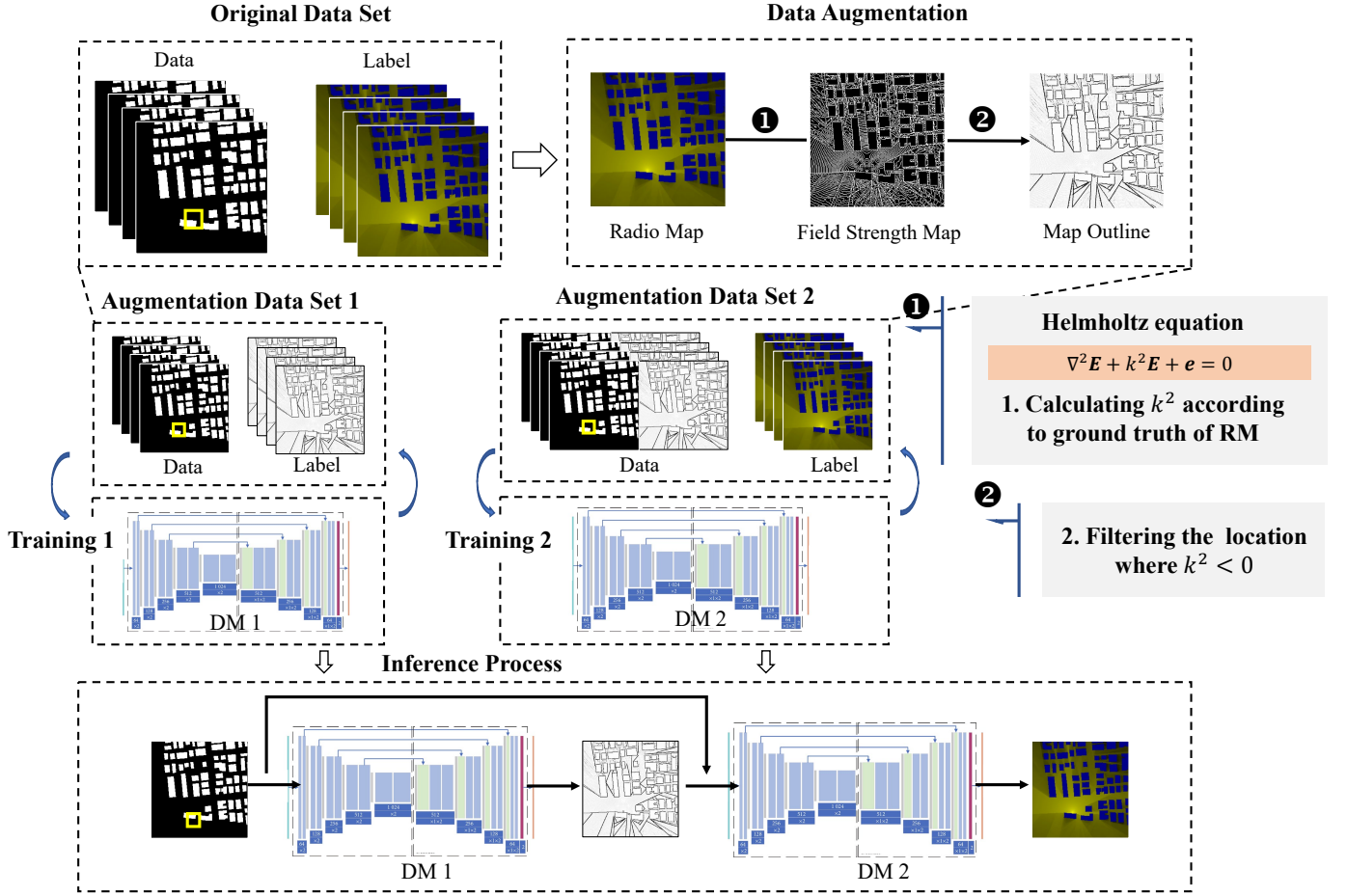


Fig. 4: The illustration of RadioDiff- $k^2$  framework

### C. Helmholtz Wave align

The derivation of the Helmholtz equation begins with Maxwell's equations in a source-free, linear, isotropic, and time-invariant medium. Consider the time-harmonic forms of Maxwell's equations with an  $e^{j\omega t}$  dependence, where  $\omega$  is the angular frequency. The two curl equations are as follows.

$$\nabla \times \mathbf{E} = -j\omega\mu\mathbf{H}, \quad \nabla \times \mathbf{H} = j\omega\epsilon\mathbf{E}, \quad (15)$$

where  $\mathbf{E}$  and  $\mathbf{H}$  denote the electric and magnetic fields, respectively, and  $\epsilon$  and  $\mu$  represent the permittivity and permeability of the medium. Taking the curl of Faraday's law,  $\nabla \times (\nabla \times \mathbf{E}) = -j\omega\mu\nabla \times \mathbf{H}$ , and substituting Ampère's law into it as follows.

$$\nabla \times (\nabla \times \mathbf{E}) = -j\omega\mu(j\omega\epsilon\mathbf{E}) = -\omega^2\mu\epsilon\mathbf{E}. \quad (16)$$

Utilizing the vector identity  $\nabla \times (\nabla \times \mathbf{E}) = \nabla(\nabla \cdot \mathbf{E}) - \nabla^2\mathbf{E}$ , and assuming a source-free medium where  $\nabla \cdot \mathbf{E} = 0$ , the equation reduces to following form.

$$\nabla^2\mathbf{E} + \omega^2\mu\epsilon\mathbf{E} = 0. \quad (17)$$

By defining the wavenumber  $k = \omega\sqrt{\mu\epsilon}$ , we obtain the vector Helmholtz equation as follows.

$$\nabla^2\mathbf{E} + k^2\mathbf{E} = 0. \quad (18)$$

For fields with a radiation source, the Helmholtz equation can be expressed as follows.

$$\nabla^2\mathbf{E} + k^2\mathbf{E} + \mathbf{e} = 0. \quad (19)$$

where  $\mathbf{h}$  is the source term.

### III. SYSTEM MODEL AND PROBLEM FORMULATION

In this paper, we consider an RM construction scenario over a discrete spatial region modeled as an  $N \times N$  grid. Each grid cell is assumed to be sufficiently small such that the pathloss within a cell remains approximately constant. Consequently, the RM can be represented by a matrix  $\mathbf{P} \in \mathbb{R}^{N \times N}$ , where each entry  $P(i, j)$  denotes the pathloss value at the corresponding grid location. Similar to [12], [13], a single BS equipped with a dipole antenna serves as the sole radiation source within this region. The antenna emits EM energy as a spherical wave, and its position is specified by the tuple  $r = \langle d_x, d_y, d_z \rangle$ , where  $d_z$  denotes the BS height and  $(d_x, d_y)$  indicates its horizontal coordinates in the grid. Since the channel characteristics between different antennas in a massive MIMO system are largely independent, the single-antenna case generalizes to multi-antenna settings by simply varying the BS position across antennas [15].

The environment comprises both static and dynamic obstacles. Static obstacles such as buildings are composed of

homogeneous materials and exhibit consistent EM reflection and diffraction behavior. Following established assumptions [10], [12], [23], the interior of a static obstacle is modeled as a total EM shield, resulting in infinite pathloss, i.e., no signal propagation. The presence of static obstacles is described by a matrix  $\mathbf{H}_s \in \mathbb{R}^{N \times N}$ , where  $H_s(i, j) = 0$  indicates the absence of a static obstacle at location  $(i, j)$ . In contrast, dynamic obstacles such as vehicles induce partial attenuation and scattering of EM waves due to their smaller physical size and lower elevation. Unlike static structures, dynamic objects do not completely block wave propagation. Their spatial distribution is encoded by the matrix  $\mathbf{H}_d \in \mathbb{R}^{N \times N}$ , with  $H_d(i, j) = 0$  denoting the absence of dynamic obstacles at grid position  $(i, j)$ .

The goal of this work is to develop a NN  $\mu_\theta(\cdot)$ , parameterized by  $\theta$ , to predict the pathloss distribution  $\hat{\mathbf{P}} \in \mathbb{R}^{N \times N}$  based on the environmental context and BS configuration. The network is trained to minimize the discrepancy between the predicted RM  $\hat{\mathbf{P}}$  and the ground truth RM  $\mathbf{P}$ , quantified by a loss function  $\mathcal{L}(\hat{\mathbf{P}}, \mathbf{P})$ . The overall RM construction task can thus be formulated as the following optimization problem:

**Problem 1.**

$$\min_{\theta} \quad \mathcal{L}(\hat{\mathbf{P}}, \mathbf{P}), \quad (20)$$

$$s.t. \quad \hat{\mathbf{P}} = \mu_\theta(\mathbf{H}_s, \mathbf{H}_d, r). \quad (20a)$$

#### IV. HELMHOLTZ EQUATION INFORMED DM FOR RM CONSTRUCTION

##### A. Features Analysis of Helmholtz align

To enable NNs to more effectively learn the spatial characteristics of EM wave propagation, it is essential to analyze the physical behavior of EM fields in the environment. In particular, the Helmholtz equation, which governs time-harmonic EM wave propagation, provides a physically grounded framework for characterizing the spatial field distribution. For a BS equipped with a dipole antenna, the radiated wavefront exhibits spherical symmetry. In such scenarios, the Laplace operator in spherical coordinates simplifies the Helmholtz equation into a one-dimensional form that captures the essential field behavior [15]. Let  $\mathbf{u}(r)$  denote the time-harmonic EM field as a function of radial distance  $r$ . The Laplacian in spherical coordinates reduces to as follows.

$$\nabla^2 \mathbf{u} = \frac{1}{r^2} \frac{d}{dr} \left( r^2 \frac{d\mathbf{u}}{dr} \right) = \frac{2}{r} \frac{d\mathbf{u}}{dr} + \frac{d^2 \mathbf{u}}{dr^2}. \quad (21)$$

Substituting into the Helmholtz equation yields the canonical form as follows.

$$\frac{d^2 \mathbf{u}}{dr^2} + \frac{2}{r} \frac{d\mathbf{u}}{dr} + k^2 \mathbf{u} = 0, \quad (22)$$

where  $k^2$  is the square of the wave number, governed by the frequency and the electromagnetic properties of the medium. The behavior of the field solution to (22) critically depends on the sign of  $k^2$ . When  $k^2 > 0$ , the solution represents a radiating wave, commonly written as follows.

$$\mathbf{u}(r) = \frac{Ae^{ikr}}{r^2}, \quad (23)$$

where  $A$  is a complex constant. Taking the squared magnitude of the field yields the electric field intensity as follows.

$$\mathbf{I}(r) \propto \left| \frac{Ae^{ikr}}{r^2} \right|^2 = \frac{|A|^2}{r^4}. \quad (24)$$

This inverse power-law decay is consistent with the Friis transmission equation in free space [27], indicating smooth, predictable pathloss behavior. Conversely, when  $k^2 < 0$ , the solution becomes exponentially decaying as follows.

$$\mathbf{u}(r) = \frac{Ae^{-\gamma r}}{r}, \quad \text{where } \gamma = \sqrt{-k^2}. \quad (25)$$

The corresponding electric field intensity can be obtained as follows.

$$\mathbf{I}(r) \propto \left| \frac{Ae^{-\gamma r}}{r} \right|^2 = \frac{|A|^2 e^{-2\gamma r}}{r^2}. \quad (26)$$

This exponential attenuation is characteristic of evanescent or heavily damped waves, typically arising near obstructions or within strongly scattering regions. These regions cause rapid spatial variations in the field strength and are directly responsible for the sharp transitions or texture features observed in radio maps. The contrast between these two regimes as the gradual decay for  $k^2 > 0$  and rapid attenuation for  $k^2 < 0$ . The above analysis offers a critical insight that the spatial regions where  $k^2 < 0$  are indicative of abrupt changes in wireless channel characteristics, such as those caused by multipath fading, shadowing, or diffraction. These transitions manifest as EM singularities, which are often overlooked or poorly captured by conventional NN-based RM construction methods. By explicitly modeling and learning the spatial distribution of  $k^2$ , particularly the regions where it is negative, we enable the NN to localize and extract high-variation features essential for accurately reconstructing pathloss distributions. This targeted, physics-informed approach significantly enhances the NN's ability to faithfully represent the underlying EM propagation dynamics, leading to more precise and generalizable RM predictions in complex environments.

##### B. Discretization Calculation of Helmholtz align

To leverage the Helmholtz equation for radio map (RM) construction, it is necessary to compute the spatial derivatives of the electric field, which is represented in discrete form in the RM. Specifically, the two-dimensional Helmholtz equation involves the Laplace operator applied to the electric field intensity  $u(i, j)$  as follows.

$$\nabla^2 u = \frac{\partial^2 u}{\partial x^2} + \frac{\partial^2 u}{\partial y^2}. \quad (27)$$

In practice, since RM data is sampled on a uniform grid, we employ finite difference methods to approximate the differential operators. For a uniform grid with spacing  $h$ , the second-order derivatives in the  $x$  and  $y$  directions are approximated using the central difference scheme as follows.

$$\frac{\partial^2 u}{\partial x^2} \Big|_{(i,j)} \approx \frac{u(i+1, j) - 2u(i, j) + u(i-1, j)}{h^2}, \quad (28)$$

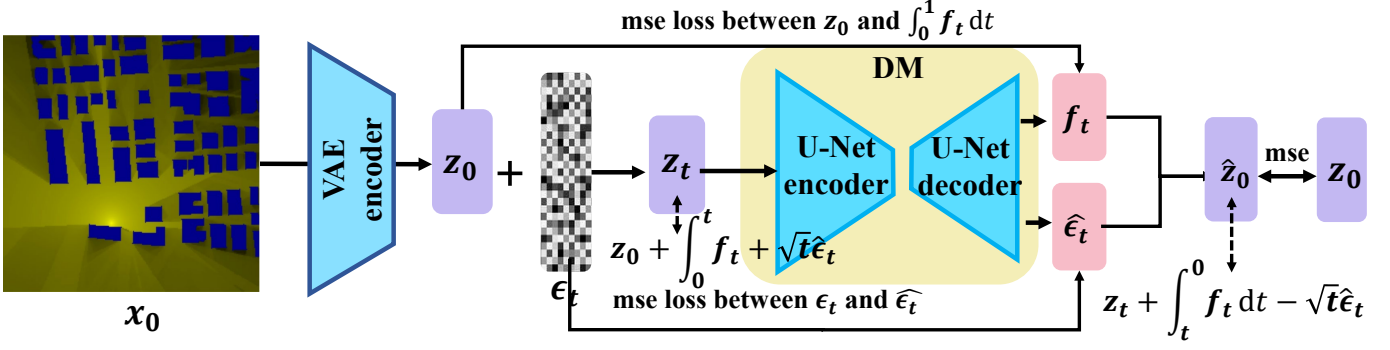


Fig. 5: The illustration of the training details.

$$\left. \frac{\partial^2 u}{\partial y^2} \right|_{(i,j)} \approx \frac{u(i, j+1) - 2u(i, j) + u(i, j-1)}{h^2}. \quad (29)$$

Similar to [28], the discrete Laplacian can be obtained as follows.

$$\begin{aligned} \nabla_h^2 u(i, j) &\approx (u(i+1, j) + u(i-1, j) \\ &\quad + u(i, j+1) + u(i, j-1) - 4u(i, j)) / h^2. \end{aligned} \quad (30)$$

This approximation is derived using Taylor series expansion and provides second-order accuracy with a truncation error of  $\mathcal{O}(h^2)$ . As the grid becomes finer (i.e.,  $h \rightarrow 0$ ), the numerical Laplacian converges to its continuous counterpart, ensuring consistency. In addition to second derivatives, gradient terms such as  $\nabla u(i, j)$  may be needed for score-based calculations or model constraints. These can also be approximated by central difference as follows.

$$\left. \frac{\partial u}{\partial x} \right|_{(i,j)} \approx \frac{u(i+1, j) - u(i-1, j)}{2h}, \quad (31)$$

$$\left. \frac{\partial u}{\partial y} \right|_{(i,j)} \approx \frac{u(i, j+1) - u(i, j-1)}{2h}. \quad (32)$$

These expressions yield a discrete gradient operator with similarly bounded error, allowing accurate evaluation of directional field changes in the RM. While these finite difference approximations allow us to evaluate the Laplacian and gradient terms, a practical obstacle remains: the RM provides only scalar pathloss values, which are proportional to the squared electric field intensity, i.e.,  $I(i, j) \propto |u(i, j)|^2$ . To recover the field magnitude suitable for Helmholtz-based modeling, we take the positive square root of RM entries. Although this transformation does not yield the absolute magnitude of the electric field, it is sufficient for identifying electromagnetic singularities—our primary interest—because, as shown in Section IV-A, such singularities correspond to regions where the wave number squared  $k^2(i, j) < 0$ . Therefore, by solving the discrete Helmholtz equation using the derived from  $\sqrt{I(i, j)}$ , we can compute the proportional form of  $k^2(i, j)$ , which retains the necessary information for locating singularities.

### C. Physics Informed Dual DM Framework

Building upon the theoretical analysis of the Helmholtz equation, we introduce Radiodiff- $k^2$ , a novel dual-stage DM

framework designed to address the complexities of RM construction, which is shown as Fig. 4. This framework draws inspiration from existing SOTA RM generation architectures but incorporates significant enhancements to leverage the underlying physics of EM wave propagation for improved performance. The architecture consists of two integral components: a Variational Autoencoder (VAE) and a Denoising UNet. The VAE's primary role is to encode the radio map from image space into a latent hidden space, which allows the denoising UNet to operate more efficiently in this compressed representation. The denoising UNet, in turn, is responsible for predicting the  $\epsilon_t$  and  $f_t$  terms required by the diffusion model during the denoising process. Moreover, the model adopts a conditional DM architecture, similar to the approach used in RadioDiff, enabling controllable RM generation based on various input conditions such as environmental features and the locations of buildings and base stations.

A key innovation of Radiodiff- $k^2$  lies in its integration of electromagnetic singularities, derived from the Helmholtz equation, to enhance RM generation. These singularities, corresponding to regions where  $k^2 < 0$ , are particularly important for accurately modeling areas of rapid change in wireless channel characteristics, such as sudden shifts in pathloss. To effectively capture these features, we designed a two-stage dual framework. In the first stage, a diffusion model is trained to learn and generate a feature map of regions where  $k^2 < 0$ , using environmental distributions and the base station location as input conditions. Once this model is trained, a second diffusion model is employed, which takes the predicted electric field singularity distribution map from the first model, along with the environmental features and base station location, to predict the final radio map.

This framework is inspired by curriculum learning [29], where the complexity of the data distribution is tackled progressively. The first diffusion model focuses on capturing regions where wireless channel features undergo abrupt changes due to electromagnetic singularities. This reduces the complexity faced by the second model, which can then use the information on the distribution of the electric field singularities to generate a more accurate radio map. This stepwise decomposition of the RM generation problem improves both the efficiency and the effectiveness of the process, ensuring that each model specializes in a distinct aspect of the radio map's

spatial characteristics. Consequently, this method not only enhances the learning of fine-grained details but also provides better generalization and scalability in dynamic and complex environments.

#### D. Training Method of RadioDiff- $k^2$

Radiodiff- $k^2$  builds upon the DDM framework, where the inference process is governed by the reverse-time stochastic differential equation defined in (14). This formulation necessitates the generative model to estimate two critical components: the deterministic drift term  $\hat{f}_t$ , which characterizes the latent trajectory of the denoising process, and the noise term  $\hat{\epsilon}_t$ , which compensates for the stochastic perturbations introduced during the forward diffusion phase. In alignment with the design paradigm of RadioDiff, the ground truth for the drift term is defined as  $\hat{f}_t = -z_0$ , where  $z_0$  denotes the clean latent representation sampled from the variational encoder.

Accordingly, we define the drift loss as the MSE between the predicted drift term and its target:

$$\mathcal{L}_{\text{drift}} = \mathbb{E}_t \left[ \left\| \hat{f}_t + z_0 \right\|_2^2 \right]. \quad (33)$$

In parallel, the noise loss is constructed as the MSE between the predicted noise component and the actual injected noise:

$$\mathcal{L}_{\text{noise}} = \mathbb{E}_t \left[ \left\| \hat{\epsilon}_t - \epsilon_t \right\|_2^2 \right]. \quad (34)$$

Meanwhile, these losses ensure that the model captures both the deterministic and stochastic components of the generative process. Although this dual-objective training strategy fosters convergence to an accurate generative path, further analysis of the reverse-time formulation offers a critical enhancement. By setting the denoising step size  $\Delta t = t$ , the model can reconstruct the clean latent variable  $\hat{z}_0$  in a single step as follows.

$$\hat{z}_0 = z_t + \int_0^t \hat{f}_\tau d\tau - \sqrt{t} \hat{\epsilon}_t. \quad (35)$$

This observation enables the incorporation of an auxiliary reconstruction loss, defined as follows.

$$\mathcal{L}_{\text{recon}} = \left\| \hat{z}_0 - z_0 \right\|_2^2, \quad (36)$$

which provides a global constraint on the learned denoising trajectory. This auxiliary term enhances training stability and promotes more faithful recovery of the latent representation, particularly under constrained denoising budgets. Combining these components, the overall loss function guiding the optimization of Radiodiff- $k^2$  is given as follows.

$$\mathcal{L}_{\text{total}} = \lambda_1 \mathcal{L}_{\text{drift}} + \lambda_2 \mathcal{L}_{\text{noise}} + \lambda_3 \mathcal{L}_{\text{recon}}, \quad (37)$$

where  $\lambda_1$ ,  $\lambda_2$ , and  $\lambda_3$  are scalar weights that balance the influence of each component. These coefficients can be tuned based on empirical performance and task-specific constraints.

Furthermore, the continuous-time formulation of the decoupled diffusion framework grants Radiodiff- $k^2$  the ability to perform adaptive-step inference. By modifying  $\Delta t$ , the model dynamically adjusts the granularity of the denoising trajectory, offering a practical trade-off between generation

fidelity and computational efficiency. In real-time applications with stringent latency requirements, coarse inference with fewer steps can be adopted, while more refined RM generation is achievable via finer denoising schedules. This operational flexibility ensures that Radiodiff- $k^2$  remains both accurate and efficient in dynamic wireless communication environments.

## V. EXPERIMENTAL RESULTS

### A. Datasets and Metrics

To rigorously assess the performance of the proposed method, we conduct experiments on three distinct datasets, each representing varying degrees of environmental complexity and electromagnetic (EM) propagation fidelity. These datasets are designed to evaluate the effectiveness of radio map (RM) reconstruction under both static and dynamic wireless scenarios, including the presence or absence of multipath effects. The foundation of our evaluation is the RadioMapSeer dataset, introduced in the Pathloss RM Construction Challenge [30]. It contains 700 uniquely structured urban maps, each incorporating between 50 and 150 buildings derived from OpenStreetMap data across cities such as Ankara, Berlin, Glasgow, Ljubljana, London, and Tel Aviv. For each map, 80 transmitter positions are specified along with the corresponding pathloss ground truth. All maps are converted into  $256 \times 256$  binary morphological images, where each pixel denotes one square meter, with ‘1’ representing building interiors and ‘0’ denoting open areas. Transmitter and receiver heights are both set to 1.5 meters, with buildings uniformly modeled at 25 meters. The transmit power is fixed at 23 dBm, and the carrier frequency is 5.9 GHz. We use 600 maps for training and 100 for testing, ensuring no terrain overlap between splits to preserve evaluation integrity. The ground truth RMs are generated by simulating EM wave propagation based on Maxwell’s equations, incorporating both reflection and diffraction. To further enhance diversity, we constructed additional datasets by varying the assumptions in the propagation models. In particular, we consider three RM variants as follows.

- Static Radio Maps (SRM), generated using the dominant path model (DPM) [31] that only accounts for the main propagation path and the influence of large-scale static buildings;
- Dynamic Radio Maps (DRM), also based on the dominant path model but additionally incorporating small-scale dynamic obstacles (e.g., vehicles) randomly distributed along roadways, thereby simulating temporal urban dynamics;
- Multipath-Aware Radio Maps (MRM), produced using an intelligent ray tracing (IRT) [17] engine that includes multipath propagation with up to four environmental interactions per signal path. Due to computational constraints, the MRM dataset excludes dynamic obstacles and focuses solely on static structures.

These three datasets collectively support a comprehensive evaluation of the proposed method, enabling us to test its ability to reconstruct high-fidelity radio maps under varying channel complexity and environmental realism.

To comprehensively evaluate the performance of RM reconstruction, we adopt a combination of classical error-based

TABLE I: **Quantitative Comparison on DPM.** Results in bold red and underlined blue highlight the highest and second highest, respectively. The  $\uparrow$  indicates metrics whereby higher values constitute improved outcomes, with higher values preferred for all other metrics.

Methods		RME-GAN	RadioUnet	RadioDiff	RadioDiff-k(Ours)	Rate(%)
SRM	NMSE	0.0096	0.0088	<u>0.0072</u>	<b>0.0043</b>	$\downarrow$ 40.28%
	RMSE	0.0279	0.0266	<u>0.0240</u>	<b>0.0193</b>	$\downarrow$ 19.58%
	SSIM $\uparrow$	0.9431	0.9466	<u>0.9560</u>	<b>0.9773</b>	$\uparrow$ 2.232%
	PSNR $\uparrow$	31.35	31.77	<u>32.67</u>	<b>34.46</b>	$\uparrow$ 5.483%
DRM	NMSE	0.0115	0.0107	<u>0.0090</u>	<b>0.0054</b>	$\downarrow$ 40.00%
	RMSE	0.0306	0.0291	<u>0.0266</u>	<b>0.0208</b>	$\downarrow$ 21.80%
	SSIM $\uparrow$	0.9276	0.9291	<u>0.9432</u>	<b>0.9704</b>	$\uparrow$ 2.884%
	PSNR $\uparrow$	30.42	30.89	<u>31.71</u>	<b>33.79</b>	$\uparrow$ 6.569%

TABLE II: **Quantitative Comparison on IRT.** Results in bold red and underlined blue highlight the highest and second highest, respectively.

Methods		RME-GAN	RadioUnet	RadioDiff	RadioDiff-k(Ours)	Rate(%)
IRT	NMSE	0.0155	0.0159	<u>0.0121</u>	<b>0.0066</b>	$\downarrow$ 45.45%
	RMSE	0.0340	0.0344	<u>0.0309</u>	<b>0.0236</b>	$\downarrow$ 23.62%
	SSIM $\uparrow$	0.9123	0.9102	<u>0.9268</u>	<b>0.9674</b>	$\uparrow$ 4.380%
	PSNR $\uparrow$	29.74	29.64	<u>30.44</u>	<b>32.68</b>	$\uparrow$ 7.352%

and perceptual quality metrics. Following previous works such as [12], we employ Normalized Mean Squared Error (NMSE) and Root Mean Squared Error (RMSE) to quantify overall prediction accuracy. However, since RM reconstruction aims not only to minimize global error but also to preserve fine structural and textural features critical to communication performance, we further incorporate Structural Similarity Index Measure (SSIM) and Peak Signal-to-Noise Ratio (PSNR) to assess perceptual and spatial fidelity.

NMSE measures the relative energy of the reconstruction error with respect to the ground truth, while RMSE reflects the square root of the averaged pixel-wise error. These metrics are defined as:

$$\text{NMSE} = \frac{\sum_{m=1}^M \sum_{n=1}^N (I_b(m, n) - I(m, n))^2}{\sum_{m=1}^M \sum_{n=1}^N I^2(m, n)}, \quad (38)$$

$$\text{RMSE} = \sqrt{\frac{1}{MN} \sum_{m=1}^M \sum_{n=1}^N (I_b(m, n) - I(m, n))^2}, \quad (39)$$

where  $I_b$  and  $I$  denote the predicted and ground truth RM values, respectively, and  $M$ ,  $N$  are the image dimensions.

To better evaluate structural fidelity, we employ SSIM, which captures perceptual similarity by considering luminance, contrast, and structural correlation between the predicted and ground truth maps. SSIM is especially relevant in RM tasks due to the presence of high-frequency textures and edge features that reflect electromagnetic wave behavior. It is computed as:

$$\text{SSIM}(x, y) = \frac{(2\mu_x\mu_y + C_1)(2\sigma_{xy} + C_2)}{(\mu_x^2 + \mu_y^2 + C_1)(\sigma_x^2 + \sigma_y^2 + C_2)}, \quad (40)$$

where  $\mu_x, \mu_y$  are the local means,  $\sigma_x, \sigma_y$  are variances, and

$\sigma_{xy}$  is the covariance between inputs  $x$  and  $y$ . Constants  $C_1$  and  $C_2$  stabilize the division and are derived from the dynamic range  $L$  of the image.

Lastly, we include PSNR to measure the reconstruction fidelity relative to the maximum possible signal intensity, with a particular focus on edge preservation, which is crucial in reflecting signal boundaries in RMs. It is defined as:

$$\text{PSNR} = 10 \log_{10} \left( \frac{r^2}{\text{MSE}} \right), \quad (41)$$

where  $r$  denotes the maximum pixel value in the image. Higher PSNR values correspond to lower reconstruction error and better visual quality. These four metrics provide a well-rounded evaluation framework, enabling both quantitative accuracy and perceptual quality assessment of radio map reconstruction performance.

## B. Comparisons with SOTA Methods

To ensure a fair and comprehensive comparison, we evaluate our proposed method against several representative deep learning-based RM construction models, each reflecting different architectural paradigms. All baseline methods are trained and tested using the same datasets and experimental settings as RadioDiff- $k^2$  to ensure consistent evaluation. The compared methods are as follows.

- **RadioUNet** [12]: A widely adopted sampling-free convolutional neural network (CNN)-based method for RM reconstruction. It leverages a U-Net architecture trained with supervised learning to infer RMs directly from environmental information. Due to its simplicity and

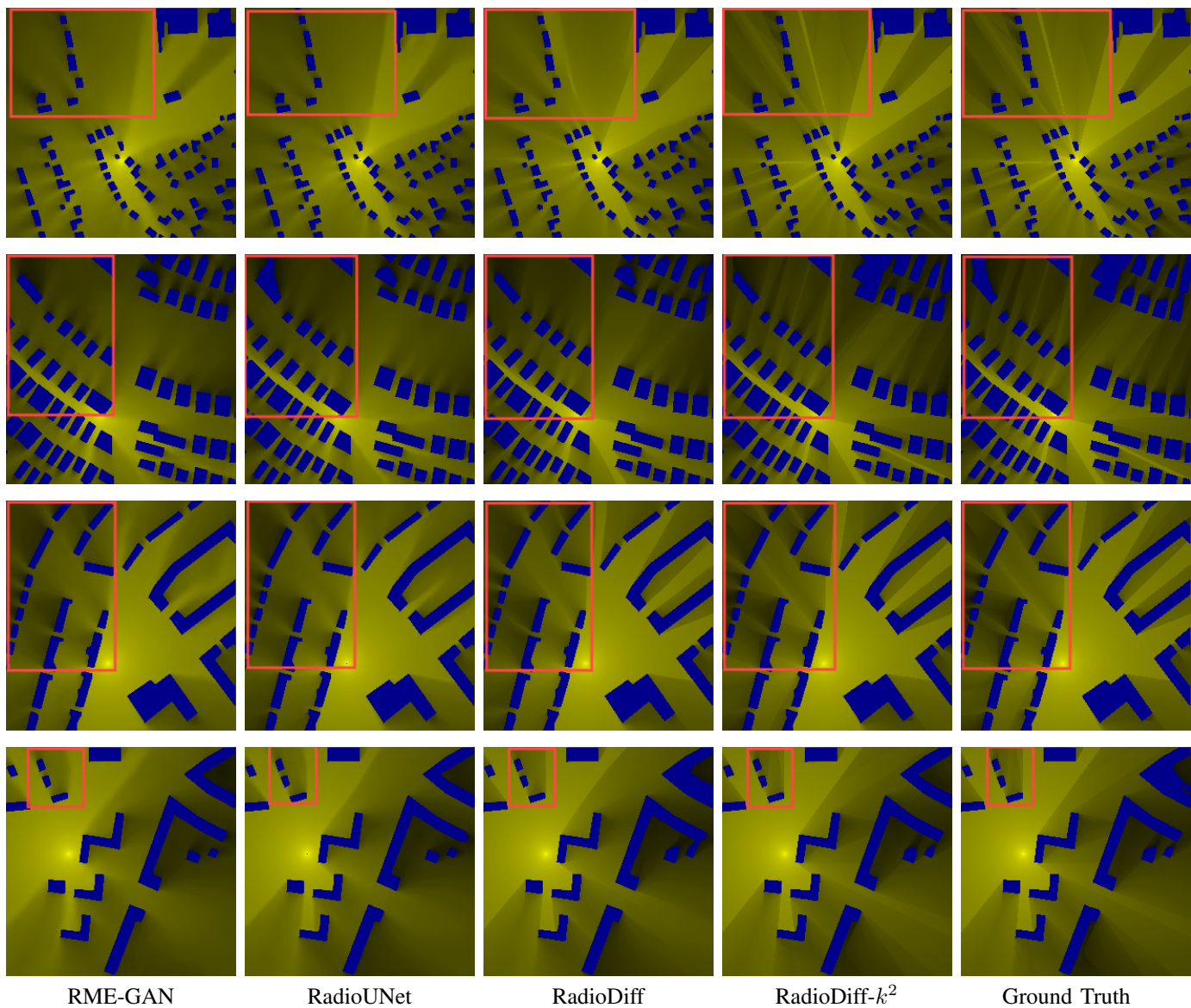


Fig. 6: The comparisons of constructed SRM on different methods.

effectiveness, RadioUNet has become a foundational benchmark in RM construction research.

- **RME-GAN** [10]: A generative adversarial network (GAN)-based model that originally incorporates both environmental features and sparse pathloss measurements (SPM) for RM generation. To ensure a fair comparison under the sampling-free setting, we adapt RME-GAN in our experiments to utilize only environmental features. While RME-GAN demonstrates the potential of adversarial training in generative RM tasks, it is not considered SOTA due to its reliance on sampled measurements in its original form.
- **RadioDiff** [13]: The current state-of-the-art in sampling-free RM construction. RadioDiff formulates the task as a conditional generative problem based on a DDM. It combines a VAE and a denoising UNet to model reverse-time EM propagation dynamics in latent space. This architecture enables fine-grained reconstruction of

pathloss textures and structural features, achieving superior performance in accuracy and perceptual quality.

### C. Evaluation on DPM

Based on the quantitative results in Table I and the qualitative comparisons in Fig. 6 and Fig. 7, the superiority of the proposed RadioDiff- $k^2$  method is clearly demonstrated across all evaluation metrics and RM types. Our method achieves substantial improvements over baseline approaches, particularly in its ability to capture fine-grained structural details and abrupt spatial variations caused by EM singularities. In the case of SRM, RadioDiff- $k^2$  reduces NMSE by over 40% compared to RME-GAN and outperforms the strong diffusion-based baseline RadioDiff by a margin of 43%. It also achieves the highest SSIM score of 0.9773, reflecting superior structural similarity, and the highest PSNR of 34.46 dB, indicating enhanced fidelity in reconstructing signal boundaries and texture features. For

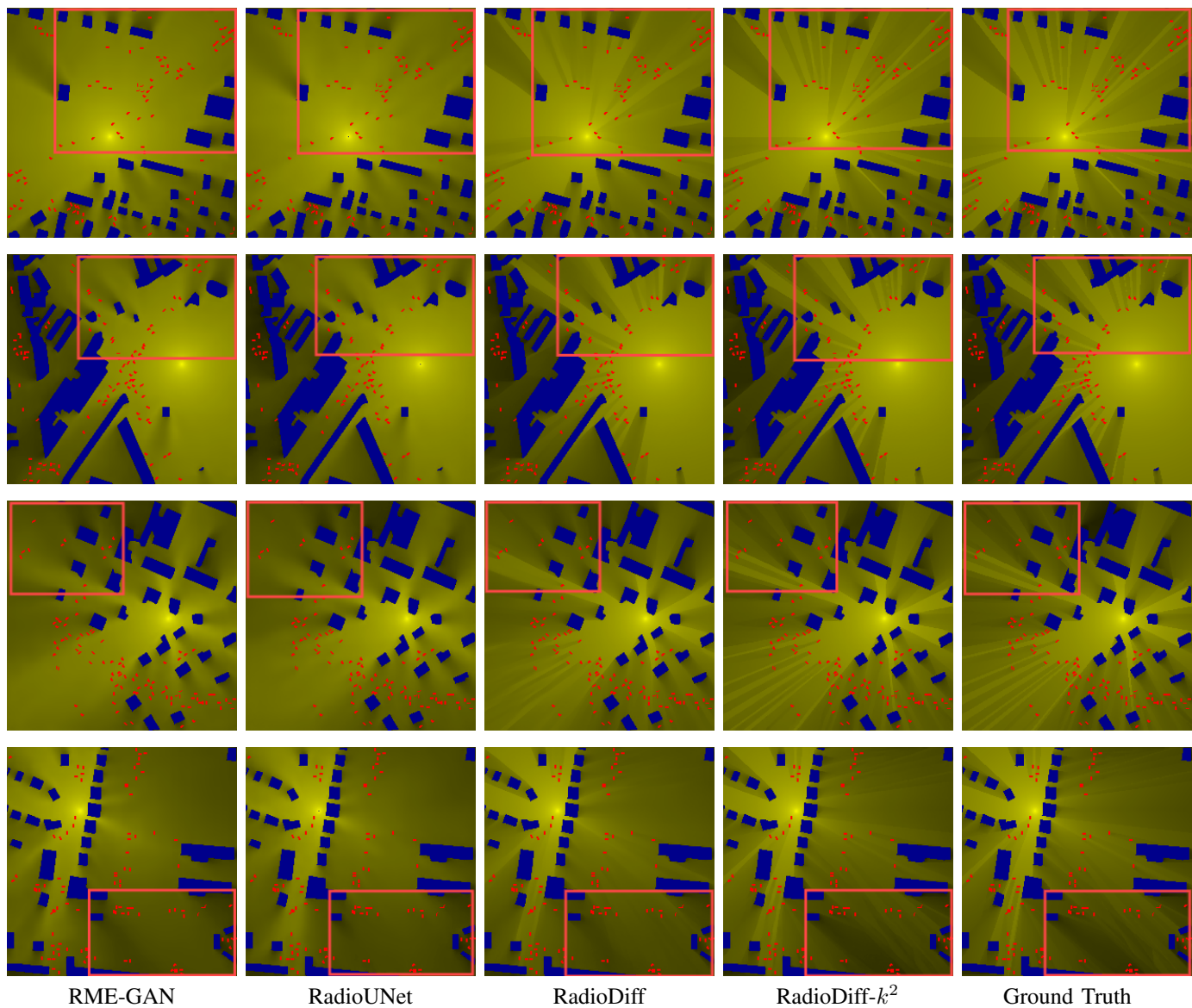


Fig. 7: The comparisons of constructed DRM on different methods. The buildings are colored blue, while the cars are colored red.

DRM, which are more challenging due to additional scattering and dynamic obstacles, RadioDiff- $k^2$  again leads with an NMSE of 0.0054, a 40% reduction from the best-performing baseline, and shows consistent gains in RMSE, SSIM, and PSNR. This indicates that our method generalizes effectively to environments with more complex propagation characteristics.

The visual comparisons further support these conclusions. As shown in Fig. 6 and Fig. 7, the RMs generated by RadioDiff- $k^2$  display significantly sharper textures, clearer signal gradients, and finer spatial transitions compared to other methods. Unlike baseline models, which often blur high-frequency structures and fail to localize abrupt changes, our approach precisely reconstructs EM singularities—regions corresponding to rapid pathloss changes induced by multipath and diffraction effects. These detailed reconstructions are crucial for real-world applications such as UAV trajectory planning and low-pilot CSI estimation, where local signal

variation must be modeled accurately. In summary, both the numerical metrics and visual results validate that RadioDiff- $k^2$  achieves state-of-the-art performance in RM reconstruction, with particularly strong advantages in modeling complex multipath and singularity-dominated scenarios.

#### D. Evaluation on IRT

Based on the results shown in Fig. 8 and the accompanying performance in Table II, our proposed RadioDiff- $k^2$  method demonstrates clear superiority over all baselines, particularly in the challenging MRM reconstruction scenario modeled using IRT4. While IRT-based datasets reflect the complex multipath propagation effects typically encountered in real-world wireless environments, they also pose significant challenges for accurate reconstruction, especially in modeling abrupt pathloss variations resulting from EM singularities. Quantitatively, RadioDiff- $k^2$

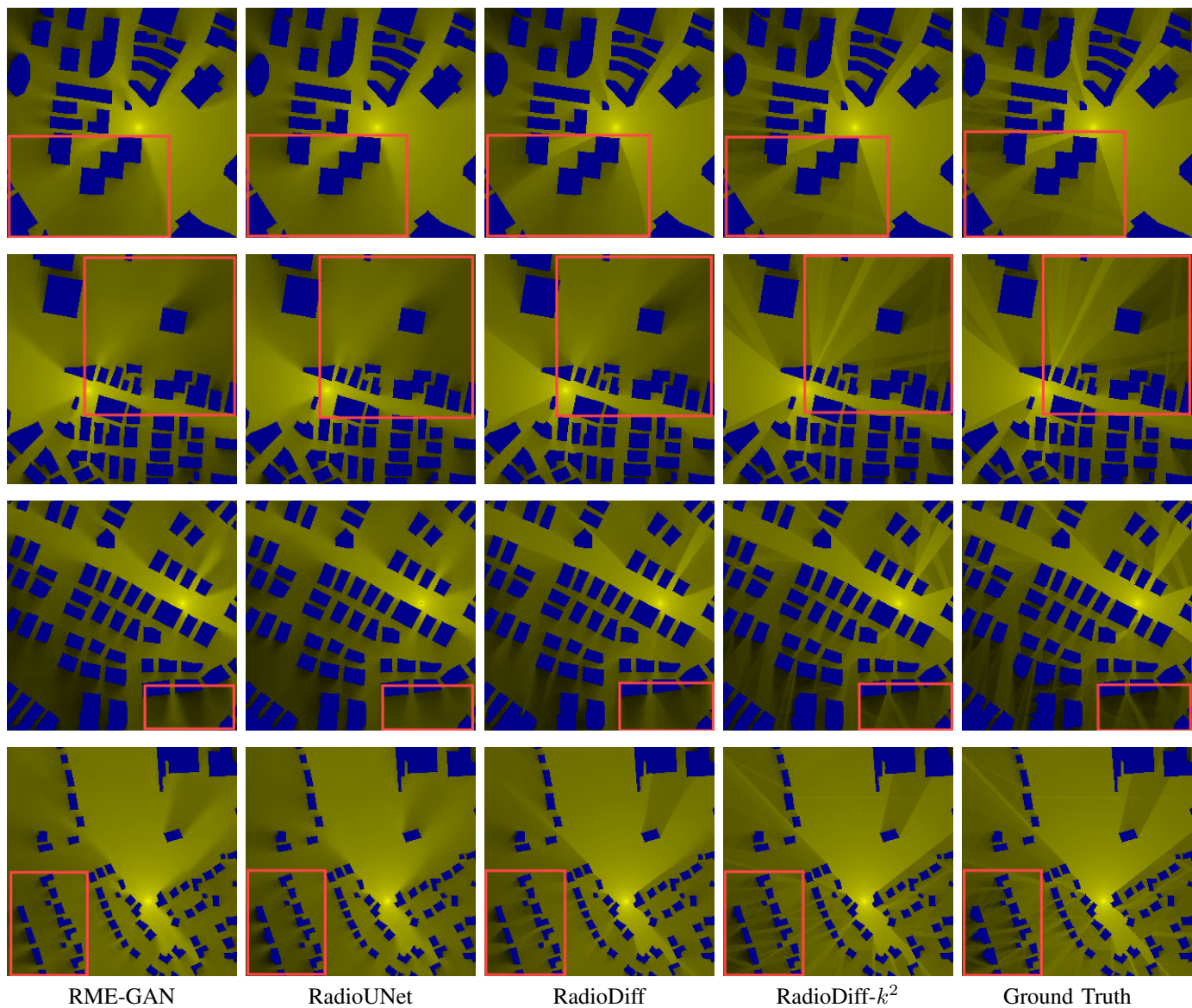


Fig. 8: The comparisons of constructed MRM on different methods.

achieves an NMSE of 0.0066, reducing the error by 45.5% compared to the best-performing baseline and significantly outperforming the standard RadioDiff. It also attains the lowest RMSE of 0.0236, and the highest SSIM of 0.9674 and PSNR of 32.68 dB scores, reflecting exceptional performance in preserving spatial structure and edge fidelity. These gains are critical in capturing high-frequency variations in EM field intensity that result from reflection, diffraction, and scattering phenomena directly linked to the distribution of EM singularities.

Visually, as shown in Fig. 8, RadioDiff- $k^2$  produces significantly sharper RM images with clearer boundaries, richer textures, and finer detail compared to existing methods. Competing baselines tend to oversmooth or blur critical signal transitions, failing to capture the multipath-induced fluctuations observable in the ground truth. In contrast, our method successfully preserves localized high-gradient regions, making it particularly well-suited for applications like trajectory planning and beam-

forming in dense and dynamic 6G environments. Overall, the results validate the effectiveness of integrating physics-based EM singularity modeling into a generative diffusion framework, establishing RadioDiff- $k^2$  as a robust and high-fidelity solution for realistic, multipath-aware RM construction.

## VI. CONCLUSION

In this work, we have proposed RadioDiff- $k^2$ , a physics-informed diffusion-based framework for accurate and multipath-aware RM construction. By incorporating the Helmholtz equation into the learning process, we have effectively identified and leveraged electromagnetic singularities—critical regions corresponding to abrupt spatial changes in wireless channel characteristics. We have further designed a two-stage generative framework that first predicts the singularity distribution and then reconstructs the RM conditioned on these fine-grained features, improving both interpretability and reconstruction

fidelity. Extensive experiments across multiple datasets, including static, dynamic, and multipath-aware environments, have demonstrated that our method significantly outperforms state-of-the-art baselines in terms of NMSE, RMSE, SSIM, and PSNR. In future work, we aim to extend our framework to 3D RM reconstruction in large-scale outdoor environments and investigate joint optimization strategies for online RM updating and trajectory planning in dynamic 6G network scenarios.

## REFERENCES

- [1] X. Shen, J. Gao, M. Li, C. Zhou, S. Hu, M. He, and W. Zhuang, "Toward immersive communications in 6G," *Frontiers in Computer Science*, vol. 4, p. 1068478, 2023.
- [2] N. Cheng, F. Chen, W. Chen, Z. Cheng, Q. Yang, C. Li, and X. Shen, "6G omni-scenario on-demand services provisioning: vision, technology and prospect(in chinese)," *Sci Sin Inform.*, vol. 54, pp. 1025–1054, 2024.
- [3] Y. Zeng and X. Xu, "Toward environment-aware 6G communications via channel knowledge map," *IEEE Wireless Commun.*, vol. 28, no. 3, pp. 84–91, 2021.
- [4] Y. Yang, M. Ma, H. Wu, Q. Yu, X. You, J. Wu, C. Peng, T. S. P. Yum, A. H. Aghvami, G. Y. Li, J. Wang, G. Liu, P. Gao, X. Tang, C. Cao, J. Thompson, K. K. Wong, S. Chen, Z. Wang, M. Debbah, S. Dustdar, F. Eliassen, T. Chen, X. Duan, S. Sun, X. Tao, Q. Zhang, J. Huang, W. Zhang, J. Li, Y. Gao, H. Zhang, X. Chen, X. Ge, Y. Xiao, C. X. Wang, Z. Zhang, S. Ci, G. Mao, C. Li, Z. Shao, Y. Zhou, J. Liang, K. Li, L. Wu, F. Sun, K. Wang, Z. Liu, K. Yang, J. Wang, T. Gao, and H. Shu, "6G Network AI Architecture for Everyone-Centric Customized Services," *IEEE Network*, vol. 37, no. 5, pp. 71–80, 2023.
- [5] Y. Zeng, J. Chen, J. Xu, D. Wu, X. Xu, S. Jin, X. Gao, D. Gesbert, S. Cui, and R. Zhang, "A tutorial on environment-aware communications via channel knowledge map for 6G," *IEEE Commun. Surveys Tuts.*, vol. 26, no. 3, pp. 1478–1519, 2024.
- [6] H. Yilmaz Birkan, T. Tugcu, F. Alagöz, and S. Bayhan, "Radio environment map as enabler for practical cognitive radio networks," *IEEE Communications Magazine*, vol. 51, no. 12, pp. 162–169, 2013.
- [7] Z. Wang, J. Zhang, H. Du, D. Niyato, S. Cui, B. Ai, M. Debbah, K. B. Letaief, and H. V. Poor, "A tutorial on extremely large-scale MIMO for 6G: Fundamentals, signal processing, and applications," *IEEE Commun. Surveys Tuts.*, vol. 26, no. 3, pp. 1560–1605, 2024.
- [8] N. Cheng, F. Lyu, W. Quan, C. Zhou, H. He, W. Shi, and X. Shen, "Space/aerial-assisted computing offloading for IoT applications: A learning-based approach," *IEEE J. Select. Areas Commun.*, vol. 37, no. 5, pp. 1117–1129, 2019.
- [9] X. Wang, L. Fu, N. Cheng, R. Sun, T. Luan, W. Quan, and K. Aldubaikhy, "Joint flying relay location and routing optimization for 6G UAV–IoT networks: A graph neural network-based approach," *Remote Sens.*, vol. 14, no. 17, p. 4377, 2022.
- [10] S. Zhang, A. Wijesinghe, and Z. Ding, "RME-GAN: A learning framework for radio map estimation based on conditional generative adversarial network," *IEEE Internet Things J.*, vol. 10, no. 20, pp. 18 016–18 027, 2023.
- [11] Z. Zheng and C. Wu, "U-shaped vision mamba for single image dehazing," *arXiv preprint arXiv:2402.04139*, 2024.
- [12] R. Levie, Ç. Yapar, G. Kutyniok, and G. Caire, "RadioUNet: Fast radio map estimation with convolutional neural networks," *IEEE Trans. Wireless Commun.*, vol. 20, no. 6, pp. 4001–4015, 2021.
- [13] X. Wang, K. Tao, N. Cheng, Z. Yin, Z. Li, Y. Zhang, and X. Shen, "RadioDiff: An effective generative diffusion model for sampling-free dynamic radio map construction," *IEEE Trans. Cognit. Commun. Networking, Early access*, pp. 1–13, 2024.
- [14] S. Oh and N.-H. Myung, "MIMO channel estimation method using ray-tracing propagation model," *Electronics letters*, vol. 40, no. 21, p. 1, 2004.
- [15] D. S. Jones, *The theory of electromagnetism*. Elsevier, 2013.
- [16] G. A. Deschamps, "Ray techniques in electromagnetics," *Proc. IEEE*, vol. 60, no. 9, pp. 1022–1035, 1972.
- [17] T. Rautiainen, G. Wölflé, and R. Hoppe, "Verifying path loss and delay spread predictions of a 3D ray tracing propagation model in urban environment," in *Proceedings IEEE 56th Vehicular Technology Conference*, vol. 4. IEEE, 2002, pp. 2470–2474.
- [18] B. Jähne, *Digital image processing*. Springer Science & Business Media, 2005.
- [19] J. Ho, A. Jain, and P. Abbeel, "Denosing diffusion probabilistic models," *Advances in neural information processing systems*, vol. 33, pp. 6840–6851, 2020.
- [20] T. Cover and P. Hart, "Nearest neighbor pattern classification," *IEEE Trans. Inform. Theory*, vol. 13, no. 1, pp. 21–27, 1967.
- [21] F. J. Breidt and J. D. Opsomer, "Local polynomial regression estimators in survey sampling," *Annals of statistics*, pp. 1026–1053, 2000.
- [22] Y. Qiu, X. Chen, K. Mao, X. Ye, H. Li, F. Ali, Y. Huang, and Q. Zhu, "Channel knowledge map construction based on a UAV-assisted channel measurement system," *Drones*, vol. 8, no. 5, p. 191, 2024.
- [23] H. Li, K. Gupta, C. Wang, N. Ghose, and B. Wang, "RadioNet: Robust deep-learning based radio fingerprinting," in *Proceedings of the 2022 IEEE Conference on Communications and Network Security (CNS)*, 2022, pp. 190–198.
- [24] G. Chen, Y. Liu, T. Zhang, J. Zhang, X. Guo, and J. Yang, "A graph neural network based radio map construction method for urban environment," *IEEE Commun. Lett.*, 2023.
- [25] Y. Song, J. Sohl-Dickstein, D. P. Kingma, A. Kumar, S. Ermon, and B. Poole, "Score-based generative modeling through stochastic differential equations," *arXiv preprint arXiv:2011.13456*, 2020.
- [26] Y. Huang, Z. Qin, X. Liu, and K. Xu, "Decoupled diffusion models: Simultaneous image to zero and zero to noise," 2024.
- [27] E. A. Lee and D. G. Messerschmitt, *Digital communication*. Springer Science & Business Media, 2012.
- [28] H. Jia, W. Chen, Z. Huang, H. Xiao, N. Jia, K. Wu, S. Lai, and Y. Yue, "Rmdm: Radio map diffusion model with physics informed," *arXiv preprint arXiv:2501.19160*, 2025.
- [29] X. Wang, Y. Chen, and W. Zhu, "A survey on curriculum learning," *IEEE Trans. Pattern Anal. Mach. Intell.*, vol. 44, no. 9, pp. 4555–4576, 2021.
- [30] Ç. Yapar, F. Jaensch, R. Levie, G. Kutyniok, and G. Caire, "The first pathloss radio map prediction challenge," in *Proceedings of the 2023 IEEE International Conference on Acoustics, Speech and Signal Processing (ICASSP)*, 2023, pp. 1–2.
- [31] R. Wahl, G. Wölflé, P. Wertz, P. Wildbolz, and F. Landstorfer, "Dominant path prediction model for urban scenarios," in *Proceedings of 14th IST mobile and wireless communications summit*, 2005, pp. 1–5.